



TECHNICAL ARTICLE

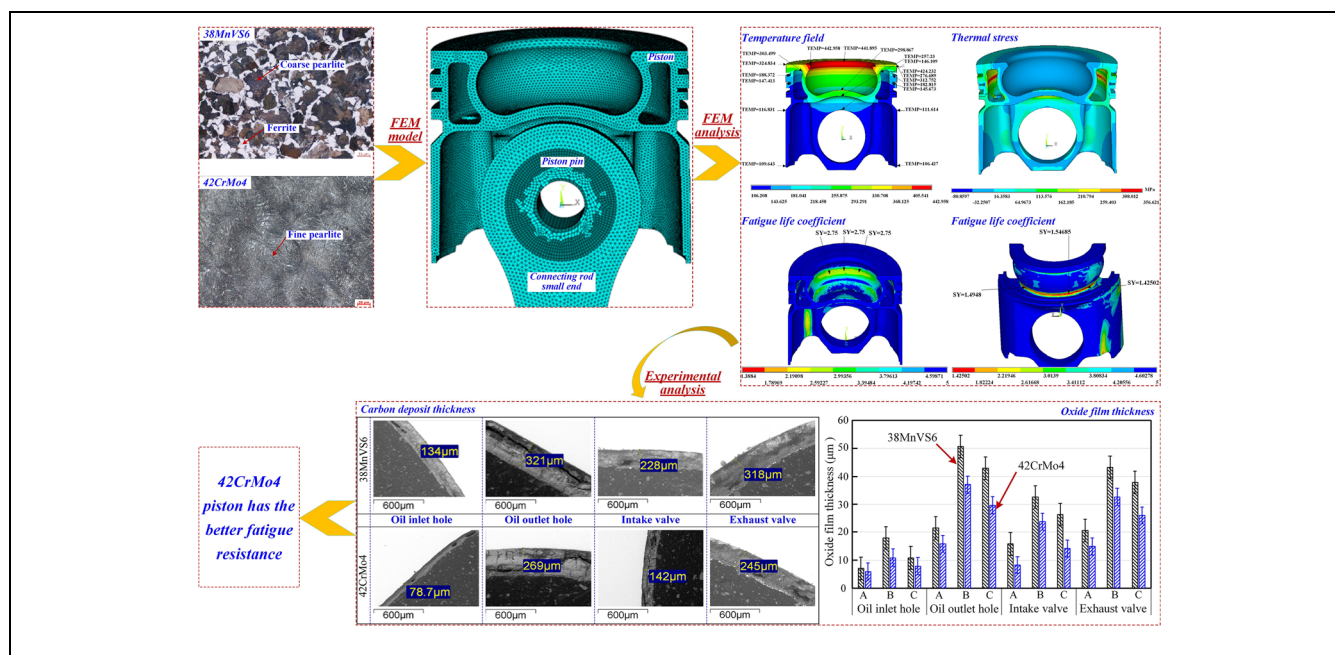
# Simulation and Experimental Investigation on Fatigue Resistance of the Forged Steel Piston in High-Duty Engine

Shaolei Gai and Jun Zhao

Submitted: 16 January 2022 / Revised: 12 July 2022 / Accepted: 22 July 2022 / Published online: 16 September 2022

Steel material is one of the necessary choices for piston to meet the high strengthening technical requirements of high-duty engines. The finite element model of piston (38MnVS6, 42CrMo4) is constructed. The temperature field, thermal stress field and fatigue safety factor of the pistons are calculated and analyzed. The piston durability experiments are carried out to investigate the influence of forging steel materials on the fatigue resistance. The results indicate that the 42CrMo4 piston has the better fatigue resistance. Under the same structure conditions, the 42CrMo4 piston achieves a smaller variation range of temperature field and 13.8% lower maximum thermal stress, compared with the 38MnVS6 piston. Moreover, the safety factor at the piston throat and at the inner cooling oil cavity is enhanced by 16 and 3%, respectively. The oxide film thickness and the carbon deposit thickness of the 42CrMo4 piston are 27 and 16% lower than that of the 38MnVS6 piston, respectively. This work provides an effective method for the selection of forged steel piston materials.

## Graphical Abstract



**Keywords** carbon deposit, fatigue resistance, FEM, forged steel, piston

## 1. Introduction

With the gradual increase in engine burst pressure, the ordinary aluminum pistons can no longer meet the technical requirements for high-strength piston of engines (Ref 1, 2). Under normal working conditions, the piston is affected by high temperature, resulting in the different temperature distribution on the piston surface. The thermal stress of different

**Shaolei Gai**, School of Mechanical Engineering, Shandong University, 17923 Jingshi Road, Jinan 250061, China; and Binzhou BoHai Positon Co., Ltd, 569 Bohai 21st Road, Binzhou 256602, China; and **Jun Zhao**, School of Mechanical Engineering, Shandong University, 17923 Jingshi Road, Jinan 250061, China. Contact e-mail: zhaojun@sdu.edu.cn.

piston materials is quite different, which affects the high-temperature fatigue resistance of the piston (Ref 3).

At present, forged steel piston is a new material product to meet the requirements of high-strength and high-power density of piston (Ref 4-7). 42CrMo4 and 38MnVS6 are widely used as piston materials, because of the excellent mechanical properties (Ref 8). The 42CrMo4 material has small Von Mises stress of 189.38 MPa and small deformation of  $5.52 \times 10^{-8}$  mm, according to the static stress analysis (Ref 9). In the manufacturing processes, the strength of the 42CrMo4 components can be improved by combining and optimizing the casting and forging (Ref 10).

With the increase in the surface temperature of the structural piston, the oxidation film would appear on the surface of the steel piston, which can lead to the oil fission of the internal cooling oil chamber of the piston and the formation of carbon deposit (Ref 11). The high-temperature gradient can induce the surface microcracks (Ref 12), which affects its service performance. Therefore, the fatigue cracks are easy to be introduced, which can reduce the fatigue resistance of the piston. On the other hand, when the engine is running, the brittle oxide film is formed on the surface of the steel piston combustion chamber at high-temperature (Ref 13-17). Under the action of high-temperature gas cycle load, the oxide film is easy to fragment and flake. The stress is concentrated at the spalling of oxide film, which results in the rapid decrease in steel strength and fatigue crack. The further crack propagation will lead to the cracking and failure of the piston combustion chamber throat. It is also found that the combination of vegetable-oil-based nanofluid MQL and surface biomimetic microstructure can effectively reduce the specific energy (Ref 18), which provides a new idea for the manufacturing of piston.

For the steel pistons, the internal cooling oil chamber is usually designed in the piston head. Carbon deposition is an important evaluation factor reflecting the fatigue of the internal cooling oil chamber in the piston (Ref 19, 20). The cooling oil oscillates through the internal cooling oil chamber. And then it takes away the heat of the piston head. During the cooling process, the oil is coking and depositing on the inner wall of the cooling oil chamber under the action of high temperature. And then a hard and rough carbon layer is formed (Ref 21, 22). The thermal conductivity of carbon deposition is about 1/50 of steel, which seriously hinders the cooling and heat dissipation of the piston head. The high-density heat of the piston combustion chamber cannot quickly escape through the cold oil chamber of the piston. At the same time, the uneven distribution of carbon deposition layer leads to the disequilibrium of heat collection in the piston head. The hot points are generated in the combustion chamber wall, which is also easily leads to fatigue failure of the piston (Ref 23).

Aiming at the high-temperature oxidation and carbon deposition problems of steel piston, the simulation and experimental investigation on fatigue resistance and oxidation resistance of the forged steels (38MnVS6, 42CrMo4) piston in high-duty engine is conducted in the work. The microstructure and mechanical properties of 42CrMo4 and 38MnVS6 piston materials were analyzed. The temperature field, thermal stress field and fatigue safety factor are investigated. Moreover, the oxide film and carbon deposition thickness of the piston are detected to evaluate the fatigue resistance and oxidation resistance of the pistons. This work provides an effective method for the selection of piston materials, and a theoretical

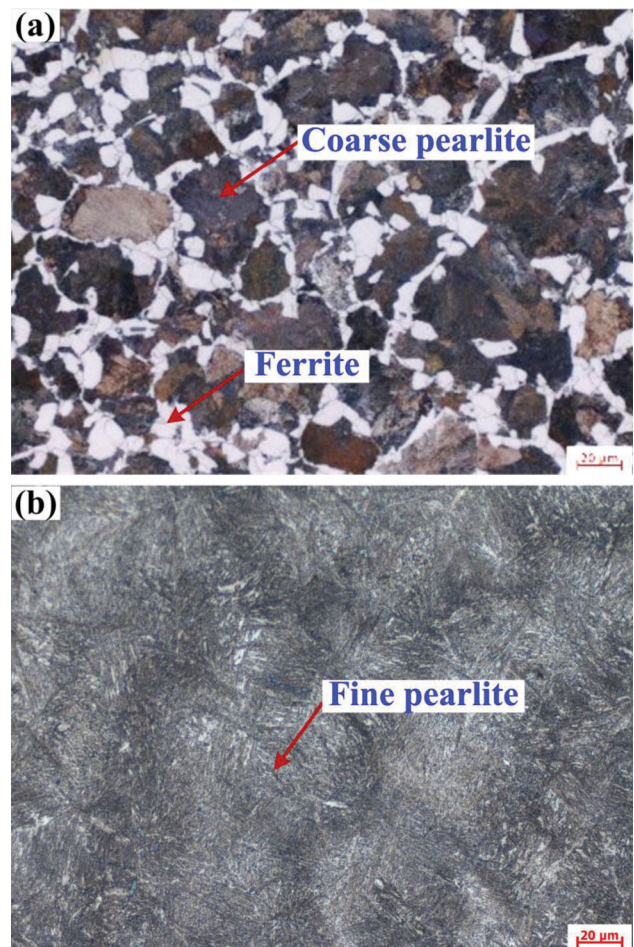


**Fig. 1** Microstructure of piston materials, (a) 38MnVS6 and (b) 42CrMo4

basis for the popularization and application of forged steel piston.

## 2. Materials and Methods

### 2.1 Piston Material

42CrMo4 alloy structural steel and 38MnVS6 alloy structural steel are used to forge piston blanks, respectively. Then, the finished piston products are processed manufactured. The microstructure of piston materials is presented in Fig. 1. 38MnVS6 material is mainly composed of coarse pearlite and ferrite, while 42CrMo4 material is mainly composed of fine pearlite. The main chemical composition and mechanical properties of the two alloy structural steel materials are shown in Table 1 and Table 2, respectively. The comparative analysis shows that the microstructure and mechanical properties of 42CrMo4 are better than those of 38MnVS6.

### 2.2 Simulation Model

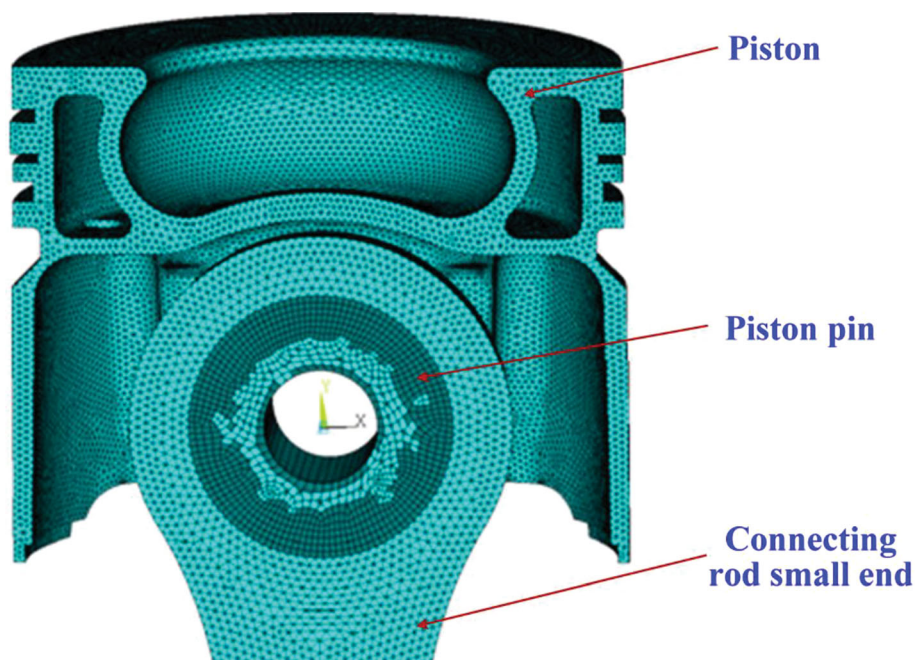
Using UG CAD software, 1/2 models of piston, connecting rod small end and piston pin are established. The 3D simulation model is presented in Fig. 2. And the symmetry constraints are defined. Piston pin hole and piston pin, connecting rod small

**Table 1 Main chemical composition of the alloy structural steels (wt.%)**

Model	C	Si	Mn	Cr	Mo	Ni	P	S	Fe
42CrMo4	0.42	0.21	0.71	1.10	0.23	0.01	0.015	0.01	Balance
38MnVS6	0.38	0.65	1.41	0.19	0.01	0.04	0.011	0.02	Balance

**Table 2 Mechanical properties of the alloy structural steels**

Model	Tensile strength, MPa	Yield strength, MPa	Reduction of area, %	Elongation, %
42CrMo4	1006 ± 35	880 ± 46	44 ± 3	14 ± 2
38MnVS6	936 ± 41	650 ± 33	40 ± 2	16 ± 2

**Fig. 2** 3D simulation model**Table 3 Main performance parameters of engine**

Cylinder bore, mm	Cylinder stroke, mm	Burst pressure, Pa	Rated power, kW	Rated speed, r/min	Total displacement, mm
135	157	169	360	1900	13.48

end and piston pin, piston skirt and cylinder liner are defined as contact constraints. Moreover, the cylinder liner is defined as full constraints. Then, the three-dimensional model is imported into ANSYS software for simulation calculation.

Both the piston and the connecting rod small end adopt second-order tetrahedron element, and the piston pin adopts hexahedron element. In order to improve the calculation accuracy, the mesh is locally densified in the parts with large temperature variation. For the piston, the number of elements is 252484 and the number of nodes is 379064. For the piston pin

and connecting rod small end, the number of elements is 327555 and the number of nodes is 541714.

Under the rated working condition of the engine, the heat exchange of the piston is in equilibrium. And the temperature field is calculated by the third boundary condition. The main simulation parameters of the engine are presented in Table 3.

### 2.2.1 Boundary Conditions of Piston Temperature Field.

- (1) Combustion chamber throat



**Table 4 Specific parameters of  $\delta_i$  and  $\lambda_i$** 

Parameter	Symbol	Value
Cylinder liner thickness	$\delta_1$	7.00, mm
Gap thickness between fire bank and cylinder liner	$\delta_2$	0.30, mm
Gap thickness between center of the 1st ring groove and cylinder liner	$\delta_3$	2.80, mm
Gap thickness between center of the 2nd ring groove and cylinder liner	$\delta_4$	2.55, mm
Gap thickness between piston skirt and cylinder liner	$\delta_5$	0.03, mm
Oil film thickness between piston ring and cylinder liner	$\delta_6$	0.01, mm
Gap thickness between piston pin and piston pin hole	$\delta_7$	0.09, mm
Thermal conductivity of cylinder liner	$\lambda_1$	36.20, W m <sup>-1</sup> K <sup>-1</sup>
Thermal conductivity of gas	$\lambda_2$	0.12 W m <sup>-1</sup> K <sup>-1</sup>
Thermal conductivity of the 1st ring	$\lambda_3$	52.00, W m <sup>-1</sup> K <sup>-1</sup>
Thermal conductivity of the 2nd ring	$\lambda_4$	52.00, W m <sup>-1</sup> K <sup>-1</sup>
Thermal conductivity of oil	$\lambda_5, \lambda_6, \lambda_7$	0.21, W m <sup>-1</sup> K <sup>-1</sup>

**Table 5 Thermal boundary conditions of key parts of the piston**

Key parts of the piston	Surrounding temperature, °C	Heat transfer coefficient, W m <sup>-1</sup> K <sup>-1</sup>
Combustion chamber throat	950	856
Fire bank	200	361
1st ring groove	200	3086
2nd ring groove	180	961
Internal cooling oil cavity	120	3200
Piston inner cavity	110	3465
Piston pin hole	200	2323
Piston skirt	150	2403

In piston combustion chamber and piston top, the highest temperature is obtained at the position of the piston combustion chamber. At the same time, the heat transfer coefficient at this position is also the largest.

The conversion formula of convective heat transfer coefficient at the piston combustion chamber throat  $h_g$  can be expressed as shown in Eq 1 (Ref 24).

$$h_g = \frac{2h_m e^{0.1\left(\frac{N}{37.5}\right)^{1.5}}}{1 + e^{0.1\left(\frac{N}{37.5}\right)^{1.5}}} \quad (\text{Eq 1})$$

where  $h_m$  is the average equivalent heat transfer coefficient of gas ( $h_m = 428 \text{ W m}^{-2} \text{ K}^{-1}$ ), and  $N$  is the distance from the piston combustion chamber throat to the piston centerline ( $N = 37.5 \text{ mm}$ ).

## (2) Fire bank, ring groove and piston skirt

When the piston fire bank and one ring groove are in contact with gas, the temperature is high. Other ring grooves and ring banks have less gas under the sealing action of piston ring. And the heat is exchanged through multi-layer flat walls through gas, ring, oil film, cylinder liner, cooling water.

The calculation formula of heat transfer coefficient of multi-layer flat wall exchange model can be expressed as shown in Eq 2 (Ref 25).

$$\frac{1}{h_n} = \sum_{i=1}^n \frac{\delta_i}{\lambda_i} + \frac{1}{h_w} \quad (\text{Eq 2})$$

where  $h_n$  is heat transfer coefficient of fire bank, ring groove, piston skirt and other parts,  $\delta_i$  is the gap thickness,  $\lambda_i$  is the thermal conductivity of intermediate material, and  $h_w$  is heat transfer coefficient between cylinder liner and cooling water ( $h_w = 12,969 \text{ W m}^{-2} \text{ K}^{-1}$ ). The specific parameters of  $\delta_i$  and  $\lambda_i$  are presented in Table 4, which is provide by Chongkang Engine Co., Ltd in China.

## (3) Piston inner cavity

The piston inner cavity is communicated with the oil pan. The upper part of the piston inner cavity is located at the bottom of the piston combustion chamber. At the same time, the bottom part of the piston inner cavity is communicated with the oil pan. The heat exchange of the piston inner cavity mainly comes from the heat at the top of the piston and the heat of the oil mist in the oil pan at the bottom of the piston. The heat at the bottom of the combustion chamber is taken away by the oil in the oil pan.

The heat transfer coefficient of the oil mist in the piston inner cavity  $h$  (Ref 26) is calculated as

$$\frac{1}{h} = \frac{(T_2 - T_n)\delta}{(T_1 - T_2)K} \quad (\text{Eq 3})$$

**Table 6 Specific working conditions of engine fatigue test**

Parameter	Value
Rotation speed	1900 ± 5, r/min
Power	360 ± 1, KW
Oil pressure	261 ± 2, kPa
Oil temperature	122 ± 1, °C
Inlet water temperature	95 ± 1, °C
Outlet water temperature	105 ± 1, °C
Inlet air temperature	24 ± 1, °C
Outlet air temperature	623 ± 2, °C
Temperature before intercooling	159 ± 2, °C
Temperature after intercooling	49 ± 1, °C
Fuel consumption	82 ± 1, kg/h

where  $T_1$  is the temperature of the piston top surface ( $T_1 = 369.8$  °C),  $T_2$  is the temperature of the piston inner cavity bottom surface ( $T_2 = 231.3$  °C),  $T_n$  is the oil mist temperature in the crankcase ( $T_2 = 130.0$  °C, which is generally the same as the oil temperature in the oil pan),  $\delta$  is the thickness between the center of the piston top combustion chamber and the bottom of the piston inner cavity ( $\delta = 7$  mm), and  $K$  is the thermal conductivity of the piston material ( $K = 42$  W m<sup>-1</sup> K<sup>-1</sup>).

The thermal boundary conditions of key parts of the piston mainly include the surrounding temperature and heat transfer coefficient of the piston combustion chamber throat, the fire bank, the 1st ring groove, the 2nd ring groove, the piston internal cooling oil cavity, the piston inner cavity, the piston pin hole, the piston skirt. According to the engine temperature field experiment and the calculation of Eq 1, 2 and 3, the thermal boundary conditions of key parts of the piston are determined, as shown in Table 5. The data in Table 5 are also provided by Chongkang Engine Co., Ltd in China.

**2.2.2 Mechanical Load.** During the working process of the piston, the mechanical load borne by the piston mainly includes the explosion pressure of gas, its own inertial force and the lateral force between piston and cylinder sleeve.

The total force applied to the piston  $F_g$  is expressed as

$$F_g = \frac{\pi D^2}{4}(P - P') \quad (\text{Eq 4})$$

where  $D$  is the diameter of piston ( $D = 135$  mm),  $p$  is the pressure exerted by the maximum explosion pressure of fuel gas in the cylinder on the piston top surface and fire bank ( $p = 17$  MPa), and  $p'$  is the gas pressure in the oil pan ( $p' = 0.1$  MPa).

The maximum reciprocating inertia force of the piston assembly  $F_j$  is expressed as

$$F_j = -m_j R \omega^2 (\cos \alpha + \lambda \cos 2\alpha) \quad (\text{Eq 5})$$

where  $m_j$  is the weight of piston assembly ( $m_j = 3658$  g),  $R$  is the radius of crank ( $R = 70$  mm),  $\omega$  is the rotation angular velocity of crank ( $\omega = 199$  rad/s),  $\lambda$  is the ratio of crank radius to connecting rod length ( $\lambda = 0.33$ ), and  $\alpha$  is crank corner ( $\alpha = 10^\circ$ ).

The lateral force on the piston  $F_N$  is expressed as

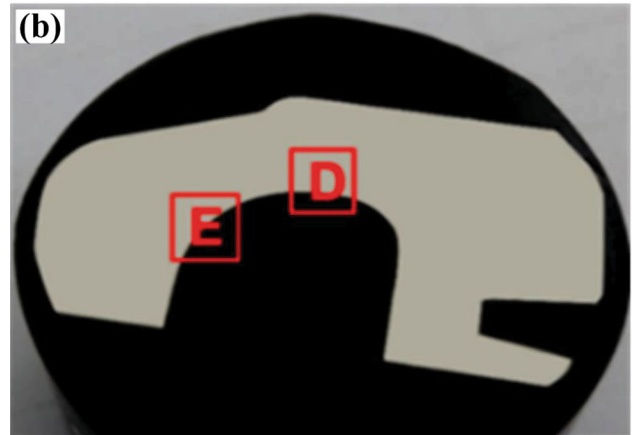
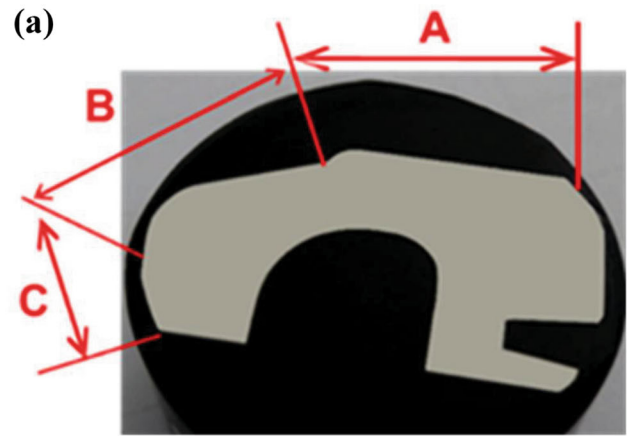


**Fig. 3** Schematic diagram of detection position, (a) Oxide film detection position and (b) Carbon deposition detection position

$$F_N = (F_g + F_j) \tan \Phi \quad (\text{Eq 6})$$

where  $\phi$  is the swing angle of the connecting rod ( $\phi = 3.32^\circ$ ).

### 2.3 Experimental Design and Method

After the 1000-h fatigue test of the engine, the engine is disassembled and the piston is taken out. The specific working conditions of engine fatigue test is exhibited in Table 6.

The oxidation degree of the piston combustion chamber and the surface carbon of the inner cooling oil cavity wall are observed. The processing method of wire cutting is adopted. And a  $t$ -shaped block is, respectively, taken from the four representative positions of the oil outlet hole, the oil intake hole, the intake valve and the exhaust valve of the piston, which is made into an insert for SEM observation (Fig. 3). As shown in Fig. 3(a), the oxide film thickness at these three locations is detected: (A) the upper part of piston combustion chamber, (B) the piston combustion chamber throat, and (C) the bottom of piston combustion chamber throat. As shown in Fig. 3(b), the carbon deposition thickness at these two locations is detected: (D) at the top of the internal cooling oil cavity and (E) at the internal cooling oil cavity corresponding to the combustion chamber throat.

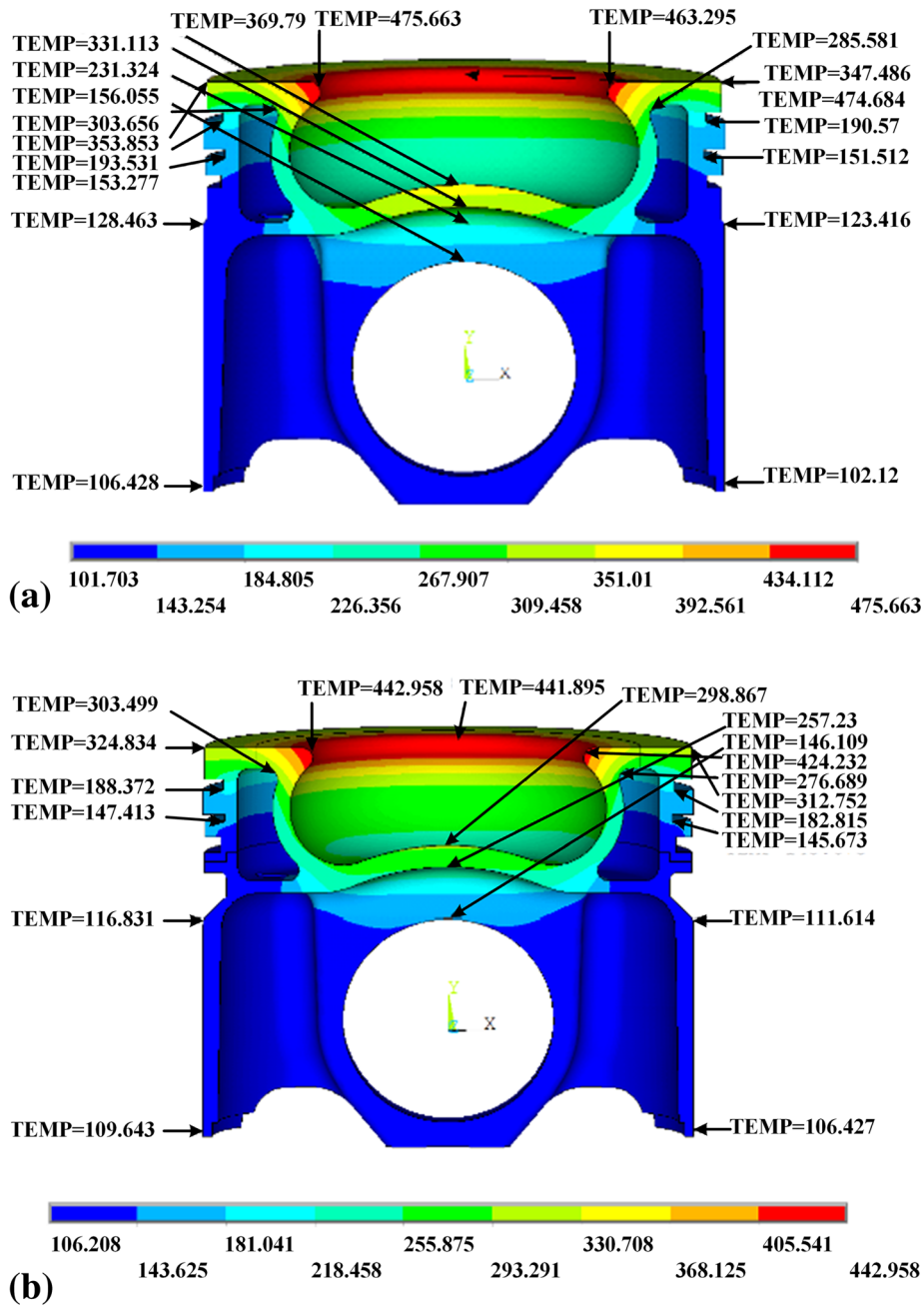


**Fig. 4** Temperature field distribution of piston, (a) 38MnVS6 and (b) 42CrMo4

The formation of high-temperature oxide film is the process of surface oxidation of piston material. The degree of oxidation reflects the anti-oxidation fatigue performance of the material. The oxide film thickness of the forged steel piston combustor is measured by scanning electron microscopy (SEM) to analyze the high-temperature fatigue characteristics of forged steel at the piston combustor throat. Then, the thickness of carbon deposits in the inner cooling oil cavity is detected, in order to compare and analyze the high-temperature fatigue properties of the forged steel material in the inner cooling oil cavity of the piston.

### 3. Results and Discussion

#### 3.1 Temperature Field and Thermal Stress Field

The temperature field distribution of pistons is exhibited in Fig. 4. The highest temperature of the piston is concentrated at the combustion chamber throat on the top surface of the piston. For the inner cooling oil cavity, the maximum temperature is concentrated at the top position of the cooling oil cavity of the piston. This position is close to the piston combustion chamber throat. With the decrease in piston height, the piston temperature is reduced gradually.

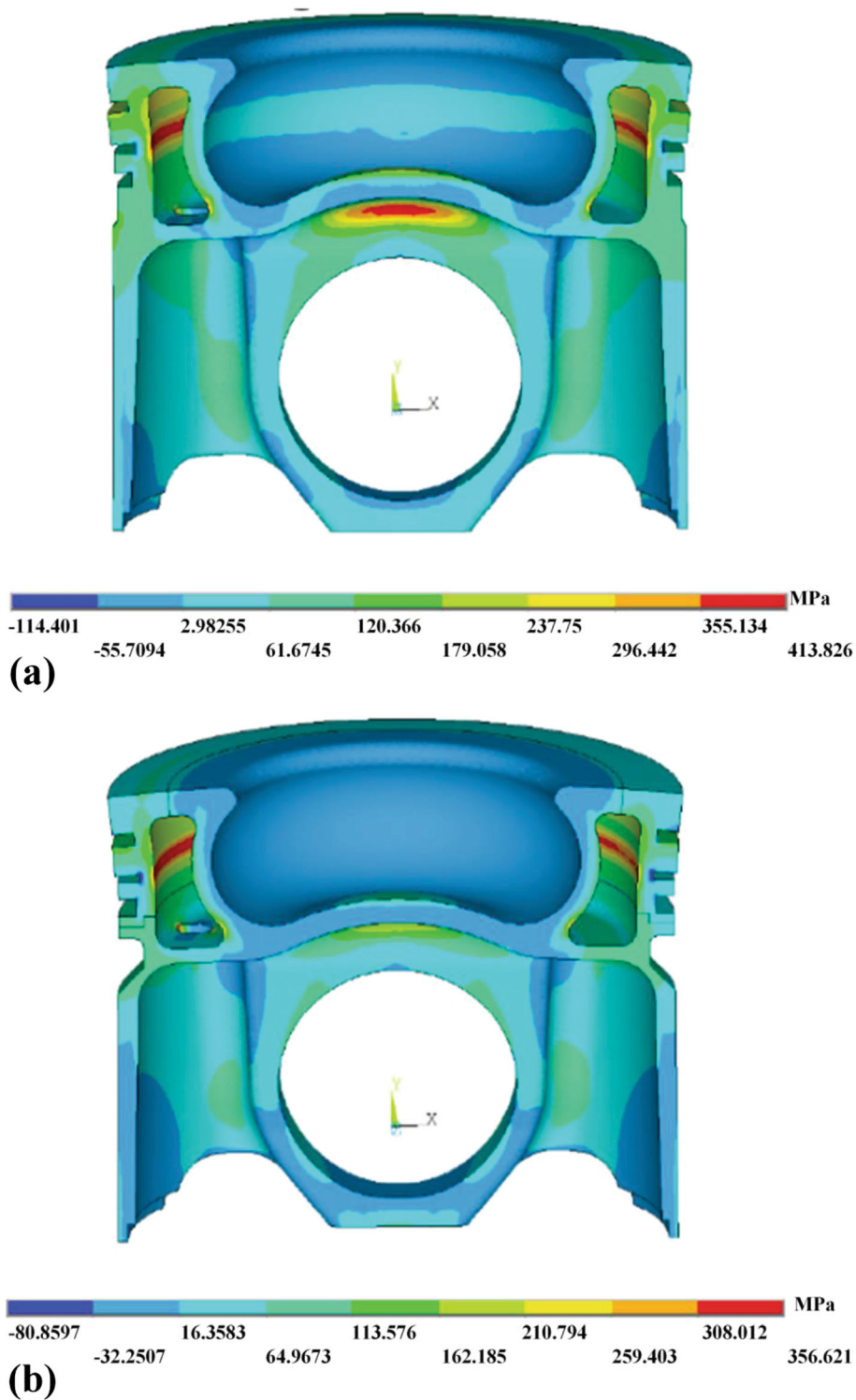


**Fig. 5** Thermal stress distribution of piston, (a) 38MnVS6 and (b) 42CrMo4

As shown in Fig. 4, the temperature range of the main part of 38MnVS6 piston is 102–476 °C, while the temperature range of the main part of the 42CrMo4 piston is 106–443 °C. The temperature distribution range of 38MnVS6 is greater than that of 42CrMo4, which can be attributed to the thermal conductivity of the two materials. Under the working conditions of the engine, the throat temperature rise of 38MnVS6 piston combustion chamber is 34 °C higher than that of 42CrMo4,

which results from the high-density heat flow of gas. Most of the heat is released by the piston ring and the cold oil chamber in the piston. At the same time, the engine cooling system causes it to cool down. Due to the dual effects of heat release and cooling, the piston skirt low-end temperature of 38MnVS6 is 4.3 °C lower than that of 42CrMo4.

The thermal stress distribution of piston is displayed in Fig. 5. Under the same working conditions of the engine, the

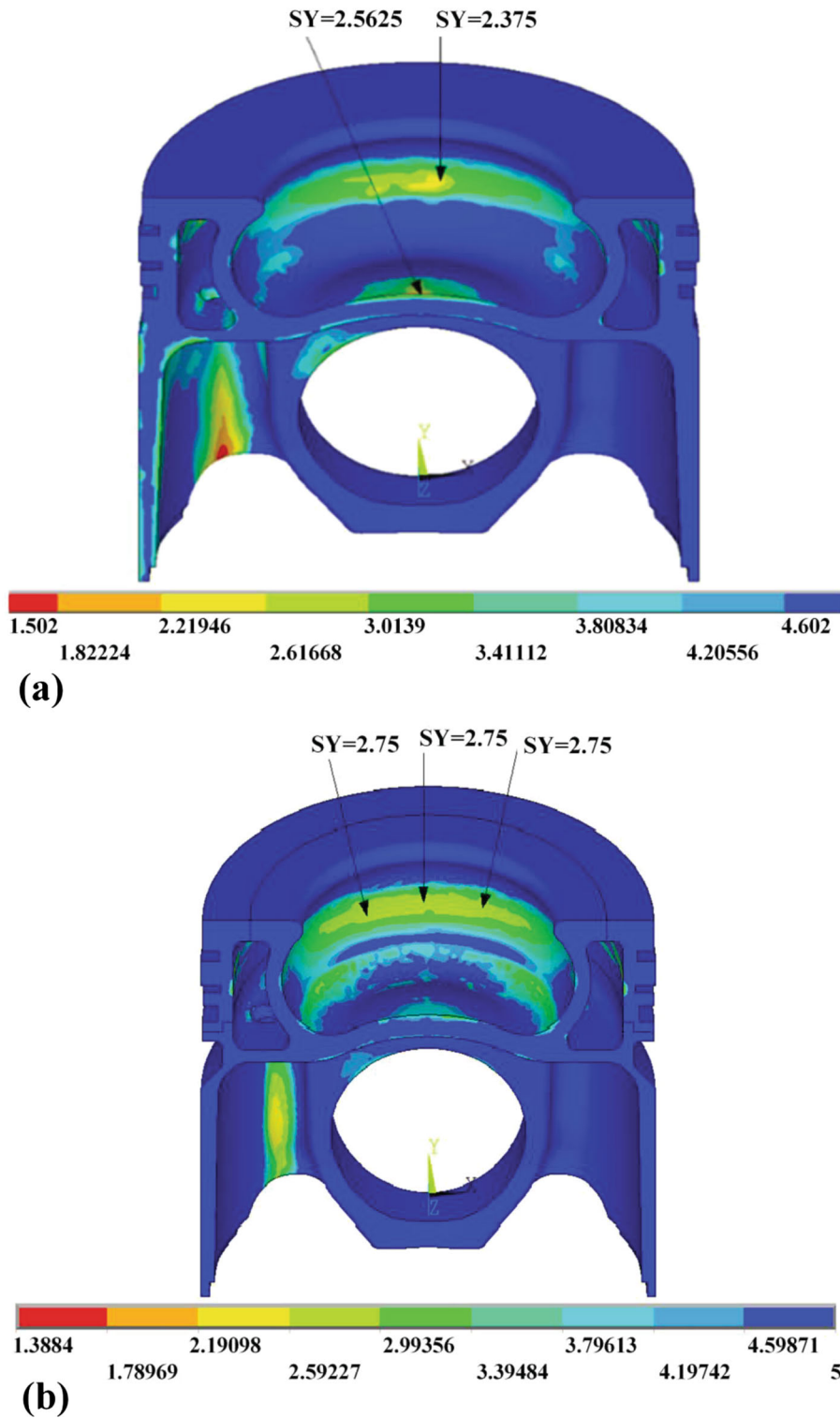


**Fig. 6** Fatigue life coefficient of piston combustion chamber, (a) 38MnVS6 and (b) 42CrMo4

temperature variation range of 42CrMo4 piston is lower than that of 38MnVS6 piston. Compared with 38MnVS6 piston, the higher mechanical properties of 42CrMo4 piston (Table 2) lead to the lower changes in thermal stress. The maximum thermal stress of 38MnVS6 piston is 414 MPa, while the maximum thermal stress of 42CrMo4 piston is 357 MPa, as shown in Fig. 5. According to the simulation calculation, the maximum

thermal stress of 42CrMo4 piston is 13.8% lower than that of 38MnVS6 piston.

### 3.2 Fatigue Life Analysis

The calculated piston temperature field and stress are imported into FEA fatigue analysis software FE-SAFE. Fatigue strength of piston material is set in the software, which is



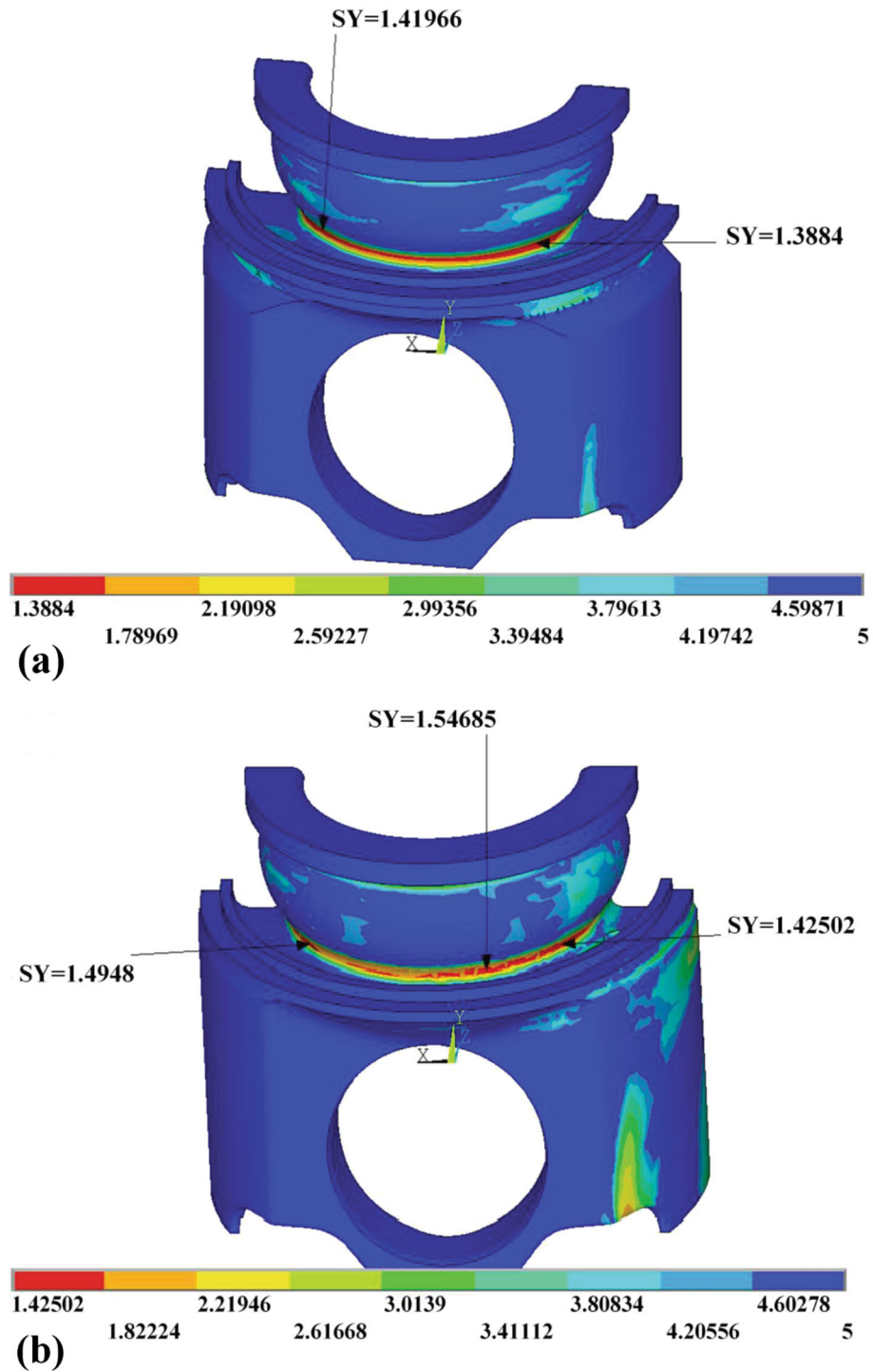


Fig. 7 Fatigue life coefficient of internal cooling oil cavity in piston, (a) 38MnVS6 and (b) 42CrMo4

Table 7 Oxide film thickness on the piston combustion chamber surface

Piston material	Oil inlet hole	Oil outlet hole	Intake valve	exhaust valve
38MnVS6	7.07-17.9, $\mu\text{m}$	21.4-50.7, $\mu\text{m}$	15.8-32.5, $\mu\text{m}$	20.5-43.2, $\mu\text{m}$
42CrMo4	5.93-10.9, $\mu\text{m}$	15.8-37.0, $\mu\text{m}$	8.28-23.7, $\mu\text{m}$	14.9-32.6, $\mu\text{m}$

measured by test. Then, the loads are applied to the model by simulating the actual working conditions of gas in the engine cylinder. And the fatigue calculation is performed. According to the Haigh type Goodman curve method (Ref 27), the fatigue life coefficient can be calculated by the maximum principal stress under the maximum working condition and the minimum principal stress under other working conditions. The fatigue life coefficient  $a$  can be obtained by the following formulas (7) and (8).

$$\sigma_a = (\sigma_{\max} + \sigma_{\min})/2 \quad (\text{Eq 7})$$

$$a = \sigma_a / \sigma_{-1f} \quad (\text{Eq 8})$$

where  $\sigma_{\max}$  is maximum principal stress under the maximum working condition,  $\sigma_{\min}$  is minimum principal stress under other working conditions,  $\sigma_a$  is the stress amplitude,  $\sigma_{-1f}$  is the fatigue strength of piston material, and  $a$  is fatigue life coefficient.

The fatigue life coefficient of the piston combustion chamber is presented in Fig. 6. The weakest fatigue performance of piston combustion chamber is located at the throat. The lowest theoretical calculation values of fatigue life coefficients of 38MnVS6 and 42CrMo4 are 2.375 and 2.75, respectively, which is higher than the empirical standard value of 1.4 of Binzhou Bohai Piston Co., LTD. It can be seen that the safety factor of forged steel piston is significantly improved. Moreover, in piston combustion chamber, the throat safety factor of 42CrMo4 is 16% higher than that of 38MnVS6. So, the fatigue resistance of 42CrMo4 piston is better in piston combustion chamber, compared with 38MnVS6 piston.

The fatigue life coefficient of internal cooling oil cavity in piston is exhibited in Fig. 7. The fatigue life coefficient of 38MnVS6 in internal cooling oil cavity is 1.3884-1.4196, while that of 42CrMo4 in internal cooling oil cavity is 1.4250-1.4948. In weakest part of the internal cooling oil cavity, the fatigue life coefficient of 42CrMo4 is 3% higher than that of 38MnVS6. In addition, the minimum fatigue life coefficient of 38MnVS6 in internal cooling oil cavity is lower than the empirical standard value (1.4) of Binzhou Bohai Piston Co., LTD., which is an unreliability factor.

The microstructure of 42CrMo4 is mainly fine pearlite (Fig. 1), resulting in its higher comprehensive mechanical properties (Table 2), especially the yield strength, compared with 38MnVS6. Under the high explosion pressure of the engine, the thermal stress of 42CrMo4 piston is lower than that of 38MnVS6 piston. The large thermal stress will damage the fatigue life of the piston. Therefore, 42CrMo4 piston has higher fatigue life coefficient and better fatigue resistance, compared with 38MnVS6 piston, as shown in Fig. 7.

### 3.3 Experimental Analysis

The piston is examined after the experiment, and oxidation is found on the surface of the piston combustion chamber at

360°. The oxide film thickness on the piston combustion chamber surface is exhibited in Table 7. Moreover, there is carbon deposition on the wall surface of internal cooling oil cavity at 360°. The carbon deposit thickness on the wall surface of internal cooling oil cavity is exhibited in Table 8.

The oxide film thickness at oil inlet hole, oil outlet hole, intake valve and exhaust valve are presented in Fig. 8. The highest thickness of oxide film thickness is obtained at outlet hole of combustion chamber. The cooling oil absorbs the heat from the top of the piston. Then the cooling effect is gradually reduced. The oil temperature at outlet hole is higher than that at oil inlet hole. Therefore, the probability of oxidation is enhanced at the oil outlet.

On the other hand, the oxide film thickness at position B is greater than that at positions A and C. This is due to the formation of vortex gas in the piston combustion chamber during the fuel combustion process. The high-temperature gas strongly swept the position of the piston combustion chamber throat, resulting in the highest temperature at this position. Therefore, the most serious oxidation of the piston material at this position is presented, which is consistent with the calculation results (Fig. 4).

As shown in Fig. 8, the oxide film thickness of 42CrMo4 piston is lower than that of 38MnVS6 piston. The oxide film thickness at position B in Fig. 3 is exhibited in Fig. 9. The oxide film thickness of 42CrMo4 piston at outlet hole B is 37.0  $\mu\text{m}$ , which is 27% lower than that of the 38MnVS6 piston (50.7  $\mu\text{m}$ ). On the one hand, the Fe+ and Cr+ elements in the 42CrMo4 piston matrix material combine with O+ to form an oxide layer. The Cr+ element in the material has better affinity for oxygen. The Cr<sub>2</sub>O<sub>3</sub> oxide layer is firstly formed on the surface of the matrix, which hinders the formation of Fe<sub>3</sub>O<sub>4</sub>. However, the content of Cr+ in 42CrMo4 material is not enough to completely form a dense Cr<sub>2</sub>O<sub>3</sub> oxide film on the substrate surface. So, some Fe<sub>3</sub>O<sub>4</sub> is still formed. On the other hand, temperature is also an important factor affecting the formation of Cr+ oxide layer. Under the working conditions of the engine, the temperature of the piston combustion chamber throat can reach 950 °C. With the increase in temperature, Cr+ element in the matrix with relatively low temperature diffuses outward. Cr<sup>3+</sup> with smaller radius gradually replaces Fe<sup>3+</sup> in the octahedral gap. Finally, the Fe<sub>3</sub>O<sub>4</sub> inverse spinel structure is transformed into the more stable FeCr<sub>2</sub>O<sub>4</sub> spinel structure. In addition, there is no antioxidant element Cr+ in 38MnVS6 piston material, which cannot prevent the oxidation of Fe+ element. Therefore, the oxide layer thickness at the combustion chamber throat of 38MnVS6 piston is relatively large.

The carbon deposit thickness at oil inlet hole, oil outlet hole, intake valve and exhaust valve are exhibited in Fig. 10. The carbon deposit thickness at position E is higher than that at position D. At the same time, the carbon deposit thickness at the internal cooling oil cavity corresponding to the combustion chamber throat (E) are serious. Due to the high temperature at

**Table 8 Carbon deposit thickness on the wall surface of internal cooling oil cavity**

Piston material	Oil inlet hole	Oil outlet hole	Intake valve	exhaust valve
38MnVS6	86.7-134, $\mu\text{m}$	275-321, $\mu\text{m}$	217-228, $\mu\text{m}$	282-318, $\mu\text{m}$
42CrMo4	56.8-78.7, $\mu\text{m}$	205-269, $\mu\text{m}$	94.0-142, $\mu\text{m}$	239-245, $\mu\text{m}$

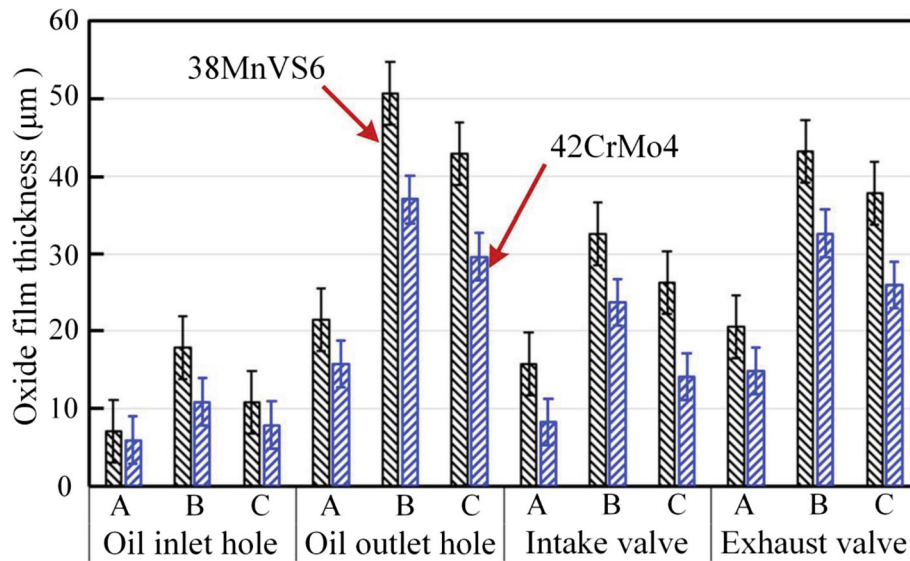


Fig. 8 Oxide film thickness at oil inlet hole, oil outlet hole, intake valve and exhaust valve

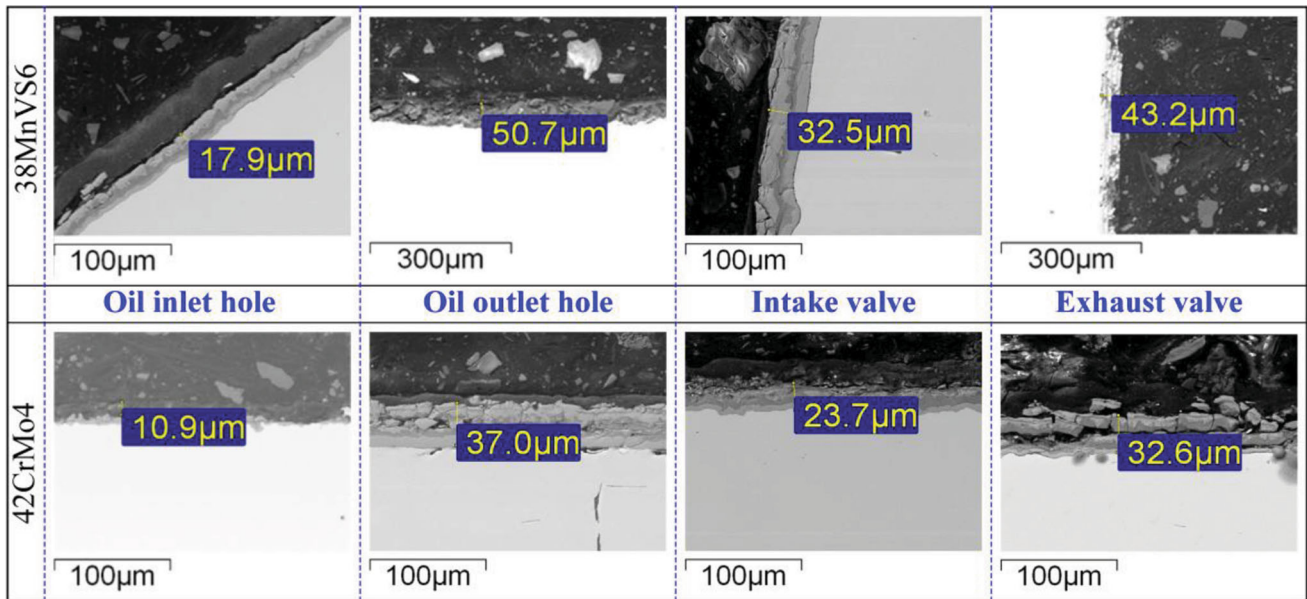


Fig. 9 Oxide film thickness at position B in Fig. 3

the piston throat, the heat conduction leads to the serious oil coking at the internal cooling oil cavity corresponding to the combustion chamber throat. Therefore, carbon deposition thickness at this position (*E*) is very high.

As shown in Fig. 10, the carbon deposit thickness of 38MnVS6 piston on the internal cooling oil cavity is significantly higher than that of 42CrMo4 piston. The carbon deposit thickness at position *E* in Fig. 3 is presented in Fig. 11. For 38MnVS6 piston, the carbon deposit thickness at oil outlet hole *E* reaches 321 μm. For 42CrMo4 piston, the carbon deposit thickness at oil outlet hole *E* is 269 μm.

The 1000-h fatigue test of the engine is carried out. According to the enterprise standard of Binzhou Bohai piston

Co., Ltd. (Q/BHS 0088-2012, Test method for engine piston performance) (Ref 28), the limit value of carbon deposition in the inner cooling oil cavity is 300 μm. The carbon deposition thickness of 38MnVS6 piston exceeds the standard value.

According to the temperature field analysis in Fig. 4, the temperature of the internal cooling oil chamber can reach about 300 °C under the working conditions of the engine. At 300 °C, the thermal conductivity of 42CrMo4 piston matrix material is 39 W/m K, while that of 38MnVS6 piston matrix material is 30 W/m K (Ref 29). The large thermal conductivity of the piston material can make the heat exchange speed of the internal cooling oil chamber fast, and promote the rapid cooling of the internal cooling oil chamber surface. Thus, the high-



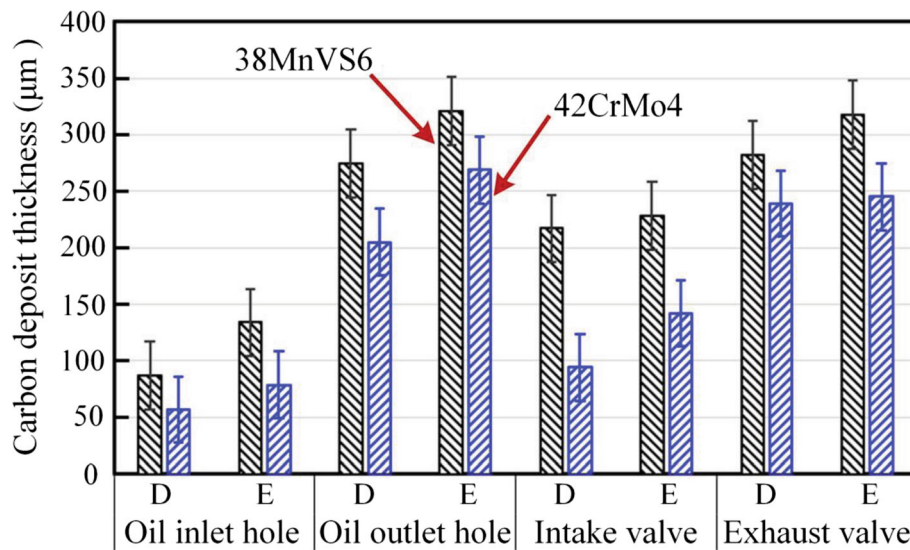


Fig. 10 Carbon deposit thickness at oil inlet hole, oil outlet hole, intake valve and exhaust valve

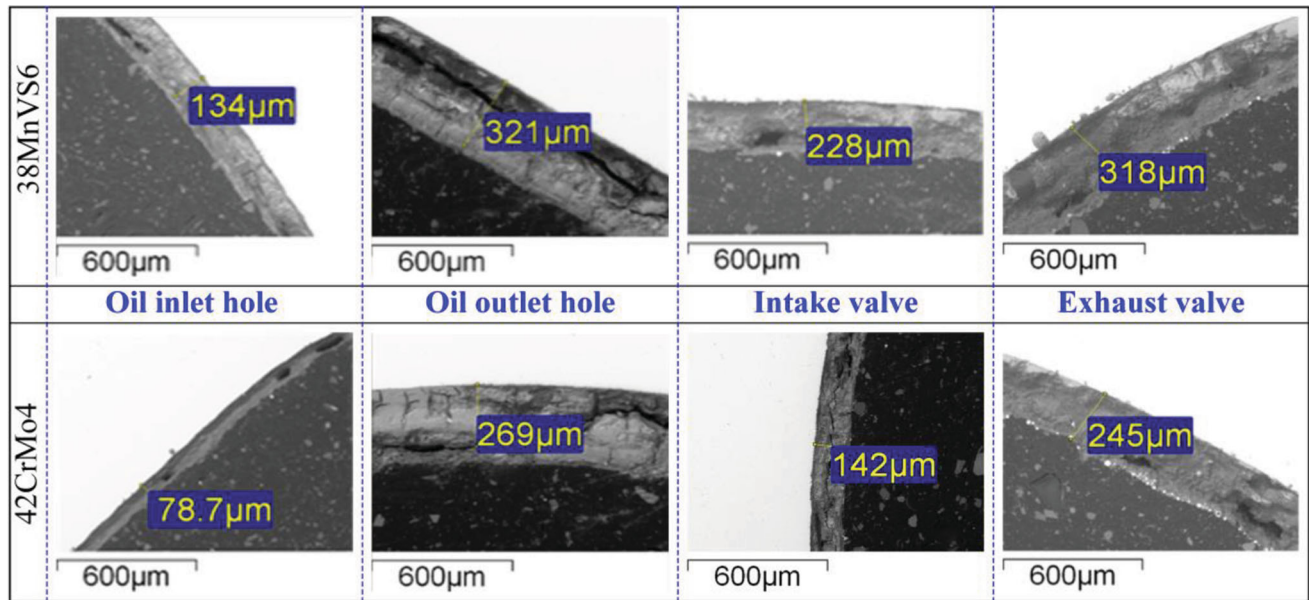


Fig. 11 Carbon deposit thickness at position E in Fig. 3

temperature coking and deposition of engine oil can be reduced. On the other hand, the uniform and dense  $\text{Cr}_2\text{O}_3$  layer is easy to form because of the chromium in 42CrMo4 piston, which can inhibit the formation of new oxide films. So, the 42CrMo4 piston surface has a relatively low carbon deposit thickness.

Compared with 38MnVS6, 42CrMo4 has more stable microstructure, stronger comprehensive mechanical properties, especially higher volume stability, under high-temperature conditions. The oxidation layer and carbon deposit layer on the surface of the 42CrMo4 material are not easy to form fatigue cracks, which can further avoid oxidation fatigue cracking at the combustion chamber throat and the inner cooling oil chamber. Therefore, 42CrMo4 forged steel has a higher fatigue resistance, which can be used for this type of piston material.

#### 4. Conclusions

- (1) The highest temperature of the piston is concentrated at the combustion chamber throat. 42CrMo4 piston has a lower temperature distribution range (106–443 °C).
- (2) The maximum thermal stress of the 42CrMo4 piston is 13.8% lower than that of the 38MnVS6 piston. The safety factor of 42CrMo4 at piston throat and at internal cooling oil cavity has a 16% and 3% higher than that of 38MnVS6, respectively.
- (3) The top surfaces of both pistons are oxidized at 360°. Moreover, the combustion chamber throat of the piston is the most severely oxidized. The oxide film thickness and carbon deposit thickness of 42CrMo4 piston are sig-



nificantly lower than those of 38MnVS6 piston, respectively.

- (4) Based on the analysis results of simulation and experiment, the fatigue resistance of the 42CrMo4 is obviously higher than that of the 38MnVS6. 42CrMo4 forged steel can be used for this type of piston material.

## Acknowledgments

This work was supported by the Major Scientific and Technological Innovation Projects in Shandong Province (No. 2019JZZY010114).

## Conflict of interest

No conflict of interest exists in the submission of this manuscript, and the manuscript is approved by all authors for publication. I would like to declare on behalf of my co-authors that the work described was original research that has not been published previously, and not under consideration for publication elsewhere, in whole or in part. All the authors listed have approved the manuscript that is enclosed.

## References

1. J. Son, M. Ha, S. Ahn, and S. Choi, Durability Design of Composite Piston in Marine Diesel Engines, *Trans. Korean Soc. Mech. Eng. A*, 2010, **34**(5), p 651–657.
2. X. Lu, Q. Li, W. Zhang, Y. Guo, T. He, and D. Zou, Thermal Analysis on Piston of Marine Diesel Engine, *Appl. Therm. Eng.*, 2013, **50**(1), p 168–176.
3. G. Xu, M. Li, Y. Zhao, Q. Chen, and X. Li, Thermal Stress and Fatigue Life Analysis of Diesel Engine Piston Based on Thermal Engine Coupling, *Chin. Intern. Combust. Engine Eng.*, 2017, **38**(2), p 96–100. **(in Chinese)**
4. S. Zeng, Development Trend of Piston Structure and Materials of Heavy Vehicle Diesel Engine, *Mod. Compon.*, 2016, **6**, p 75–77. **(in Chinese)**
5. N. Uchida and H. Osada, A New Piston Insulation Concept for Heavy-Duty Diesel Engines to Reduce Heat Loss from the Wall, *SAE Int. J. Engines*, 2017, **10**(5), p 2565–2574.
6. Z. Jian and H. Li, Influence of Manganese Phosphating on Wear Resistance of Steel Piston Material under Boundary Lubrication Condition, *Surf. Coat. Technol.*, 2016, **304**, p 530–536.
7. J. Zhang, M. Li, X. Zhao, and L. Ma, Thermal Analysis of Diesel Engine Forged Steel Piston Based on Finite Element Method, *Intern. Combust. Engine Power Plant*, 2018, **2**, p 77–81. **(in Chinese)**
8. J. Su, X. Qiu, F. Xing, and R. Ye, Effect of Preheating Temperature on Microstructure and Properties of 42CrMo4/38MnVS6 Heterogeneous Laser Welded Joint, *Metals*, 2019, **9**(8), p 870.
9. Y. Basavaraj, R. Joshi, G.R. Setty, M. Samiullah, M. Museb, M. Tayab, and H. Banu, FEA of NX-11 Unigraphics Modeled Connecting Rod Using Different Materials, *Mater. Today Proc.*, 2021, **46**, p 2807–2813.
10. L. Krüger, E. Jentsch, L. Brunke, A. Keßler, G. Wolf, T. Lehnert, N. Schubert, A. Wagner, and D. Landgrebe, Development of an Innovative Lightweight Piston through Process Combination “Casting-Forging,” *Procedia Manufacturing*, 2019, **27**, p 172–176.
11. A. Baberg, M. Freidhager, H. Mergler, and K. Schmidt, Aspects of Piston Material Choice for Diesel Engines, *MTZ Worldw.*, 2012, **73**(12), p 26–30.
12. X. Cui, Y. Guo, J. Guo, and P. Ming, Performance Analysis of Laser-Induced Biomimetic Ceramic Tools in Interrupted Cutting, *Int. J. Mech. Sci.*, 2020, **177**, p 105589.
13. X. Li and X. Zhu, Cracking Analysis of Throat of a Steel Piston Combustion Chamber, *Intern. Combust. Engines*, 2020, **4**, p 36–39. **(in Chinese)**
14. M. Caldera, J.M. Massone, and R.A. Martinez, Failure Analysis of a Damaged Direct Injection Diesel Engine Piston, *J. Fail. Anal. Prev.*, 2017, **17**(5), p 979–988.
15. O. Barrau, C. Boher, R.B. Gras, and F. Rezai-Aria, Analysis of the Friction and Wear Behaviour of Hot Work Tool Steel for Forging, *Wear*, 2003, **255**(7–12), p 1444–1454.
16. X. Cui, S. Wang, Q. Jiang, and K. Chen, Research on Thermal Wear of Cast Hot Forging Die Steel Modified by Rare Earths, *J. Rare Earths*, 2007, **25**(1), p 88–92.
17. S. Wang, K. Chen, X. Cui, Q. Jiang, and B. Hong, Effect of Alloying Elements on Thermal Wear of Cast Hot-Forging Die Steels, *J. Iron. Steel Res. Int.*, 2006, **13**(5), p 53–59.
18. X. Cui, Y. Guo, J. Guo, and P. Ming, Bio-Inspired Design of Cleaner Interrupted Turning and its Effects on Specific Cutting Energy and Harmful Gas Emission, *J. Clean. Prod.*, 2020, **271**, p 122354.
19. L. Witek, Failure and Thermo-Mechanical Stress Analysis of the Exhaust Valve of Diesel Engine, *Eng. Fail. Anal.*, 2016, **66**, p 154–165.
20. X. Zhang, X. Zeng, X. Sun, B. Deng, G. Peng, H. Xie, Z. Wu, and T. Xiao, Thermal and Elemental Analysis of the Combustion Chamber Deposits in a Large-Scale Two-Stroke Marine Diesel Engine, *Sci. China Technol. Sci.*, 2015, **58**(10), p 1717–1725.
21. L. Deng, Z. Wang, and Y. Liu, Effect of Structural Parameters on Filling Rate of Closed Internal Cooling Oil Cavity, *J. Cent. South Univ. (Sci. Technol.)*, 2017, **48**(8), p 2224–2230. **(in Chinese)**
22. X. Zhang, G. Peng, G. Du, X. Sun, G. Jiang, X. Zeng, P. Sun, B. Deng, H. Xie, and Z. Wu, Investigating the Microstructures of Piston Carbon Deposits in a Large-Scale Marine Diesel Engine Using Synchrotron X-Ray Microtomography, *Fuel*, 2015, **142**, p 173–179.
23. Y. Li, Causes and Preventive Analysis of Carbon Deposition in Diesel Engine, *China South. Agric. Mach.*, 2020, **51**(14), p 2. **(in Chinese)**
24. X. Wang, *Study on Piston Heat Load of zb4e150d Engine*, Shenyang University of Technology, Shenyang, 2007. **(in Chinese)**
25. Y. Wang, Y. Liu, H. Shi, 2010, Simulation and Analysis of Thermo-Mechanical Coupling Load and Mechanical Dynamic Load for a Piston. In 2010 Second International Conference on Computer Modeling and Simulation, IEEE, 4: 106–110
26. X.F. Liu, Y. Wang, and W.H. Liu, Finite Element Analysis of Thermo-Mechanical Conditions Inside the Piston of a Diesel Engine, *Appl. Therm. Eng.*, 2017, **119**, p 312–318.
27. Y. Wang and J. Zhang, Research on Wheel Fatigue Strength Evaluation Method Based on Improved Goodman Curve, *J. Railw. Sci. Eng.*, 2017, **14**(4), p 827–832. **(in Chinese)**
28. Q/BHS 0088-2012, Test method for engine piston performance, Shandong Binzhou Bohai piston Co., Ltd., 2012
29. G. Mahle, Motorische Erprobung, In Kolben und motorische Erprobung. Vieweg+Teubner, 2011, 115–269

**Publisher's Note** Springer Nature remains neutral with regard to jurisdictional claims in published maps and institutional affiliations.